IEEE Access
Multidisciplinary | Rapid Review | Open Access Journal

Received April 8, 2021, accepted April 19, 2021, date of publication April 26, 2021, date of current version May 3, 2021.

Digital Object Identifier 10.1109/ACCESS.2021.3075499

A Synchronized Current Difference Updating Technique for Model-Free Predictive Current Control of PMSM Drives

CRESTIAN ALMAZAN AGUSTIN[1], JEN-TE YU[2], YU-SHAN CHENG[1], (Member, IEEE), CHENG-KAI LIN[1], AND YA-WEI YI[1]

[1]Department of Electrical Engineering, National Taiwan Ocean University, Keelung City 202, Taiwan
[2]Department of Electrical Engineering, Chung Yuan Christian University, Taoyuan City 32023, Taiwan

Corresponding author: Cheng-Kai Lin (cklin@mail.ntou.edu.tw)

This work was supported by the Ministry of Science and Technology, Taiwan, under Grant MOST-109-2221-E-019-022-MY2.

ABSTRACT Model-free predictive current control (MFPCC) is a promising substitute for model predictive current control (MPCC). However, the performance of the MFPCC, to a large extent, hinges on the update frequency of its lookup table. Conventionally, the update is only performed when two successive switching states applied by the controller are identical, causing a stagnation problem to the current difference of those switching states that are not applied. To address the stagnation problem, this paper proposes a novel mechanism called synchronized current difference update for model-free predictive current control (SCDU-MFPCC). The presented scheme uses the model of permanent-magnet synchronous motor (PMSM) to construct equivalent differential stator currents corresponding to seven basic voltage vectors. To that end, current slope will be defined from the current difference of two successively applied voltage vectors. An updating factor associated with the current slope is then introduced into the prediction scheme to correct the enforced response of all switching states. This scheme is applied on every current measurement to update the stored information regardless of the successive switching states applied are distinct or not. Finally, experiments are conducted to assess the performance of the new approach using a TMS320F28379D microcontroller. Experimental results demonstrate that the proposed method substantially reduces the stagnation effect under steady-state and dynamic operations.

INDEX TERMS Current slope, model predictive current control, model-free, permanent-magnet synchronous motor, synchronized current difference update.

I. INTRODUCTION

Nowadays, most electric drives are often equipped with AC induction machines (IM) or permanent magnet synchronous motors (PMSM). IM drives are commonly used because of their availability and cost-effectiveness, but it lags fairly behind efficiency and performance than the PMSM [1], [2]. As a result, the PMSM drive is considered a more practical choice for traction and other industrial applications. However, to exploit these advantages, the PMSM requires an advanced controller to operate, on which several control strategies have been proposed and employed [3]–[6].

Among them, the model predictive current control (MPCC) has been regarded as an ideal control scheme [7]. With several inherent advantages of fast dynamic response, real-time implementations, and nonlinearly constrained control, the performance can be significantly improved [8], [9]. It offers an ideal substitute for the conventional PI controllers and hysteresis comparators, thanks to the rapid development of modern high-speed microcontrollers [10], [11]. As MPCC is model-based, its success is anchored on the model of the motor. In other words, the accuracy of current prediction is highly dependent on the system parameters, which are affected by several factors, such as load changes, skin effects, and operating temperature variations, to name just a few [12]–[14]. MPCC is known to be sensitive to parameter mismatches and perturbations that may lead to performance degradations [15]–[17].

Various approaches have been presented to address the issue. Ren *et al.* [18] adopted an estimator for uncertainties

The associate editor coordinating the review of this manuscript and approving it for publication was Pinjia Zhang.

and disturbances by updating the parameters online, but the current control scheme therein was PI-based. In [19], an adaptive feedforward speed control strategy is proposed to compensate for the nonlinear components and parameter uncertainties. A real-time parameter updating mechanism is also presented by Zhang *et al.* [20] for parameter estimation of the MPCC to yield good performance. However, the computational burden makes it less practical due to its complex control design. Moreover, studies have shown that the reduced observer strategy can pose risks in terms of system stability, accuracy, and complexity [21], [22].

A totally different strategy, which is model-free, was first applied to motor drives by Lin *et al.* [23], [24]. The model-free predictive current control (MFPCC) has successfully mitigated the difficulties caused by parameter sensitivity and model dependence of the conventional MPCC. The progress of the MFPCC has been observed in many motor drive applications, including the PMSM [22] and other variants, such as the surface-mounted PMSM (SPMSM) [21] and interior PMSM (IPMSM) [23]. Their implementations effectively boosted the performance of the machine by improving system robustness [21], reducing torque ripples [22], and enhancing the current tracking responses [23]. Generally, with the conventional MFPCC, current measurements are made and stored in a lookup table (LUT) over a switching interval. However, with only two current detections in a sampling period and low update frequency [23], the LUT suffers from a current stagnation problem, making the stored data obsolete and problematic. The issue has been addressed by [24], which imposes a refresh rate window at a predefined sampling period. Although the current stagnation problem is resolved, applying a non-optimal switching state after the refresh window can still adversely affect the system performance. The authors of [25] and [26] have respectively proposed a novel anti-stagnation technique by reconstructing the current differences relative to the stored information of their lastest three voltage vectors applied. The approximation strategy is innovative in suppressing the stagnation effect, but its implementation is very demanding that requires calculations of the switching vectors' angular displacement and active application moments.

In this paper, a significant update to [23] and [24] is presented with a simplified synchronized update mechanism of current differences. Each of the seven base voltage vectors is updated in real-time without extensive calculations. Instead, the update corresponding to each voltage vector is defined by their correlations. The implementation is simple and can be realized by algorithms that are computationally much less demanding.

The contributions of this paper are highlighted as follows:

1. Incorporate a novel and simplified synchronized current difference update (SCDU) into the conventional MFPCC, which is termed SCDU-MFPCC, in the sequel.
2. The SCDU-MFPCC is anchored on the model of the PMSM to construct the differential stator currents of the seven base voltage vectors.
3. Unlike [23] and [24], the update frequency of the SCDU-MFPCC is implemented in real-time. Current difference is updated upon the current detection to prevent LUT stagnation.
4. Updating factors are introduced into the predictive algorithm to correct and update the enforced response of the current slope of two applied switching states.
5. Experiments are performed to assess the performance of the proposed SCDU-MFPCC over the conventional MFPCC under steady-state and dynamic settings.

The rest of the paper is organized as follows. Section II presents a brief overview of MPCC. Section III discusses the limitations of MFPCC. Section IV proposes the synchronized updating technique. Experimental validation is provided in Section V, and finally, a conclusion is provided in Section VI. Appendices are also given, featuring mathematical analysis and derivations of the differential stator currents of selected switching states.

II. THE MPCC AND THE MOTOR DRIVES

An overview of the application of MPCC to the permanent-magnet synchronous motor (PMSM) drives is provided in this section. It includes the machine model, current prediction mechanism, and cost function as a measure of current prediction error.

A. MACHINE EQUATIONS OF PMSM

Compared to other AC motors, PMSM is electromechanically simpler, thanks to the equal dq inductances. To further simplify the mathematical model, some assumptions are made, including 1) negligible magnetic saturation, 2) sinusoidal back-EMF, 3) insignificant effect of magnetic hysteresis loss, eddy current loss, and clogging torque, and 4) symmetrical and balanced three-phase winding.

The stator voltage equation of PMSM in the stationary $\alpha\beta$ reference frame can be written as

$$\begin{cases} v_s = R_s i_s + \dfrac{d\psi_s}{dt} \\ \quad = R_s i_s + L_q \dfrac{di_s}{dt} + \dfrac{d\psi_r}{dt} \\ \quad = R_s i_s + L_q \dfrac{di_s}{dt} + e_s \end{cases} \tag{1}$$

where v_s, R_s, i_s, ψ_s, ψ_r, L_q, and e_s are stator voltage vector, stator resistance, stator current vector, stator flux vector, equivalent rotor flux vector, q-axis inductance, and equivalent back-EMF, respectively.

B. CURRENT PREDICTION, DELAY COMPENSATION, AND BACK-EMF ESTIMATION

By rearrangement of (1), the stator current equation can be derived as follows:

$$\frac{di_s}{dt} = \frac{1}{L_q}\left(v_s - R_s i_s - e_s\right). \tag{2}$$

Since (2) is a first-order differential equation, a simple approximation can be obtained by a finite difference technique. That is, through an Euler approximation, di_s/dt can

be approximated by

$$\frac{di_s}{dt} \approx \frac{i_s(k+1) - i_s(k)}{T_s} \tag{3}$$

where T_s is the sampling period, $i_s(k+1)$ and $i_s(k)$ are the sampled stator currents at $(k+1)th$ and $(k)th$ periods, respectively. Given (2)-(3), one can obtain the discrete expression of the predicted stator current as

$$i_s^p(k+1) = \left(1 - \frac{R_s T_s}{L_q}\right) i_s(k) - \frac{T_s}{L_q}\left(v_s(k) - e_s(k)\right). \tag{4}$$

It can be observed from (4) that the prediction horizon is one step from the commanding period of the applied voltage vector. Typically, a delay is inherently present in digital implementations due to sampling and filtering. As such, the control at $(k)th$ period may not be the best to apply. Instead, a two-step compensation scheme [27] is adopted. The current predictions at $(k+2)$ time steps can be expressed as

$$i_s^p(k+2) = \left(1 - \frac{R_s T_s}{L_q}\right) i_s(k+1) - \frac{T_s}{L_s}\left(v_s(k+1) - e_s(k)\right). \tag{5}$$

Given the fact that the sampling is fast enough for modern digital signal processors, the back-EMF can be assumed to be constant within two successive sampling intervals, namely, $e_s(k) \approx e_s(k+1)$.

C. COST FUNCTION AS A MEASURE OF ERROR

The objective of the MPCC is to minimize the error between the current command and predictions of (5). The prediction error is commonly expressed in orthogonal coordinates of $\alpha\beta$, representing the real and imaginary parts of the current vectors. With a single control applied in the cost function, the weighting factors can be eliminated, making it more advantageous and straightforward. As a measure of error, the cost function is defined as

$$J_{S_h} = \left|i_\alpha^{ref}(k+2) - i_\alpha^p(k+2)\right|^2 + \left|i_\beta^{ref}(k+2) - i_\beta^p(k+2)\right|^2 \tag{6}$$

where i_α^{ref} and i_β^{ref} represent the reference currents, and the subscript S_h denotes any of the candidate switching states, where $h \in \{0, 1, 2, 3, ...6\}$. The value of the cost function serves as a criterion to select the optimal voltage vector yielding minimum prediction error. In this paper, a six-switch three-phase inverter module is used that generates seven switching states, as shown in Table 1. The control of the MPCC is illustrated in Fig. 1.

III. THE MFPCC

The model-free predictive current control (MFPCC) is proposed to eliminate model dependence and mitigate the effect from parameter perturbations [23]. The stator currents are measured directly from motor terminals through current sensors.

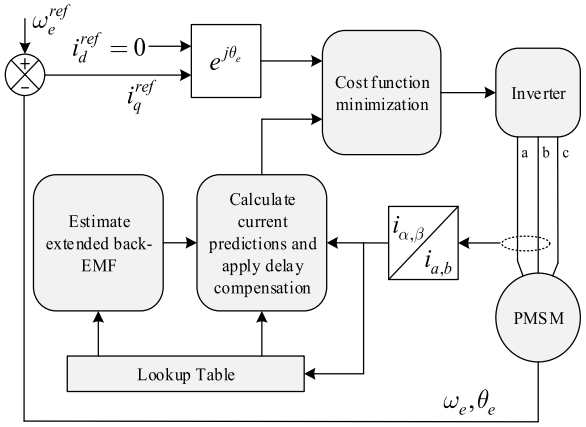

FIGURE 1. The block diagram of a conventional MPCC.

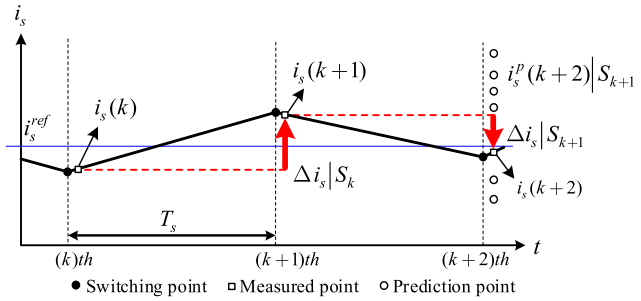

FIGURE 2. Current prediction of conventional MFPCC.

As depicted by Fig. 2, the stator current measurements at time k are on α and β axes and denoted as $i_\alpha(k)$ and $i_\beta(k)$. A short delay is purposefully introduced between the switching and prediction to avoid measurement of current spikes from the arching of power switches. After prediction, the current measurement will be made alongside the current differences between successive switching intervals. The values are then stored in the LUT *via* the microcontroller.

For instance, the current difference at time $k+1$ can be calculated from the stator currents sampled at $(k)th$ and $(k+1)th$ intervals. Namely, they are written as

$$\begin{cases} \Delta i_\alpha\,|\,S_k = i_\alpha(k+1) - i_\alpha(k) \\ \Delta i_\beta\,|\,S_k = i_\beta(k+1) - i_\beta(k). \end{cases} \tag{7}$$

Similarly, one may have the following

$$\begin{cases} \Delta i_\alpha\,|\,S_{k+1} = i_\alpha(k+2) - i_\alpha(k+1) \\ \Delta i_\beta\,|\,S_{k+1} = i_\beta(k+2) - i_\beta(k+1). \end{cases} \tag{8}$$

Given current differences, the prediction can be made as follows:

$$\begin{cases} i_\alpha^p(k+2)\,|\,S_{k+1} = i_\alpha(k) + \Delta i_\alpha\,|\,S_k + \Delta i_\alpha\,|\,S_{k+1} \\ i_\beta^p(k+2)\,|\,S_{k+1} = i_\beta(k) + \Delta i_\beta\,|\,S_k + \Delta i_\beta\,|\,S_{k+1}. \end{cases} \tag{9}$$

One may observe from (9) that current predictions are independent of model parameters. However, its outcome hinges on how frequently the information of the LUT is updated. Low update frequency may result in the so-called stagnation effect.

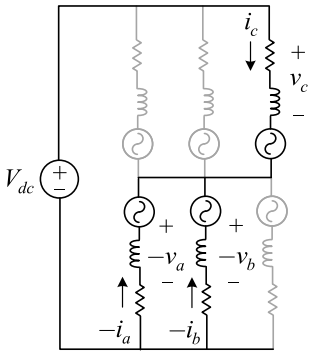

FIGURE 3. Equivalent circuit diagram of switching state S_5 with switching combination of (001).

With modern high-speed microcontrollers, the sampling frequency can be conveniently set to be very high, allowing certain assumptions to be made. Suppose the switching states applied between two successive intervals are the same, the variation of their current differences is assumed negligible. As such, $\Delta i_\alpha | S_k$ and $\Delta i_\beta | S_k$ can be expressed as follows:

$$\begin{cases} \Delta i_\alpha^{old} \Big| S_k \approx \Delta i_\alpha \Big| S_k \\ \Delta i_\beta^{old} \Big| S_k \approx \Delta i_\beta \Big| S_k \end{cases} \tag{10}$$

where the superscript *"old"* refers to the previous current difference of the same switching state stored in the processor. The assumption, however, is only valid when the same switching modes are applied in succession. In other words, the current differences stored from other switching states may suffer from a stagnation problem if they become idle or have not been used for certain intervals. The stagnation may lead to inaccurate current predictions. To resolve this drawback, a programmed update frequency with a refresh window of 50ms is enforced in [24]. After the refresh, the LUT is automatically updated by a new applied switching state. However, the method misses the crucial selection of optimal switching state that may affect the ultimate prediction accuracy and performance.

IV. A SYNCHRONIZED CURRENT DIFFERENCE UPDATE FOR MFPCC

A novel synchronized current difference update for MFPCC is presented in this section. The PMSM model is utilized to define current differences corresponding to each switching state, and Mathematica® is used to carry out the synthesis.

A. MODELING OF THE SCDU

Take S_5 as an example for modeling and analysis. Illustrated in Fig. 3 is an equivalent circuit diagram of the six-switch three-phase inverter corresponding to the switching combinations of (001). The following equations are from Kirchoff's voltage law,

$$V_{dc} = v_c - v_a \tag{11}$$

$$v_a = v_b \tag{12}$$

TABLE 1. The seven basic switching states.

Switching States	Inverter Switching	v_a	v_b
S_0	(000)/(111)	0	0
S_1	(100)	$2V_{dc}/3$	0
S_2	(110)	$V_{dc}/3$	$\sqrt{3}V_{dc}/3$
S_3	(010)	$-V_{dc}/3$	$\sqrt{3}V_{dc}/3$
S_4	(011)	$-2V_{dc}/3$	0
S_5	(001)	$-V_{dc}/3$	$-\sqrt{3}V_{dc}/3$
S_6	(101)	$V_{dc}/3$	$-\sqrt{3}V_{dc}/3$

where V_{dc}, v_a, v_b, and v_c are the dc-link voltage and the stator voltages, respectively. Note that equations (11) and (12) are described in the *abc* (three-phase) coordinates, the transformation of which to $\alpha\beta$ orthogonal coordinates can be found in the Appendices.

The vector expression of switching state S_5 in the $\alpha\beta$ coordinates are written as

$$\begin{bmatrix} \frac{di_\alpha}{dt}\Big|_{S_5} \\ \frac{di_\beta}{dt}\Big|_{S_5} \end{bmatrix} = A \begin{bmatrix} -V_{dc} \\ -V_{dc} \end{bmatrix} - A \begin{bmatrix} (2i_a - i_b - i_c) R_s \\ (-i_b - i_c) R_s \end{bmatrix} - A \begin{bmatrix} \lambda_\alpha \\ \lambda_\beta \end{bmatrix} \tag{13}$$

where A is the equivalent inductance vector and $[\lambda_\alpha \ \lambda_\beta]^T$ is the equivalent phase-wise back-EMF vector whose definitions are given as (14) and (15), shown at the bottom of the next page, where L_s and L_{ls} are the armature inductance and leakage inductance, respectively. The λ_m is the maximum rotor magnetic flux and θ_e is the electrical rotor position.

The same principle holds for other switching states as well. Hence each of them will produce a unique stator current equation.

Consequently, the equivalent differential stator current of the zero voltage vector can be expressed as follows:

$$\begin{bmatrix} \frac{di_\alpha}{dt}\Big|_{S_0} \\ \frac{di_\beta}{dt}\Big|_{S_0} \end{bmatrix} = -A \begin{bmatrix} (2i_a - i_b - i_c) R_s \\ (-i_b - i_c) R_s \end{bmatrix} - A \begin{bmatrix} \lambda_\alpha \\ \lambda_\beta \end{bmatrix}. \tag{16}$$

The zero voltage vector S_0 in (16) is found to have no V_{dc} component, implying that the influence of the dc-link is negligible. As can be seen from Table 1, the same can be observed from the switching combinations of (000) and (111). In this case, the zero voltage vectors can be considered the natural response of the stator currents. The natural response is dependent on the component of stator currents and load speeds. The V_{dc} component given in (13) is referred to as enforced response [25].

Since the proposed prediction scheme is nonparametric and model-free, (13) and (16) can be regarded as current

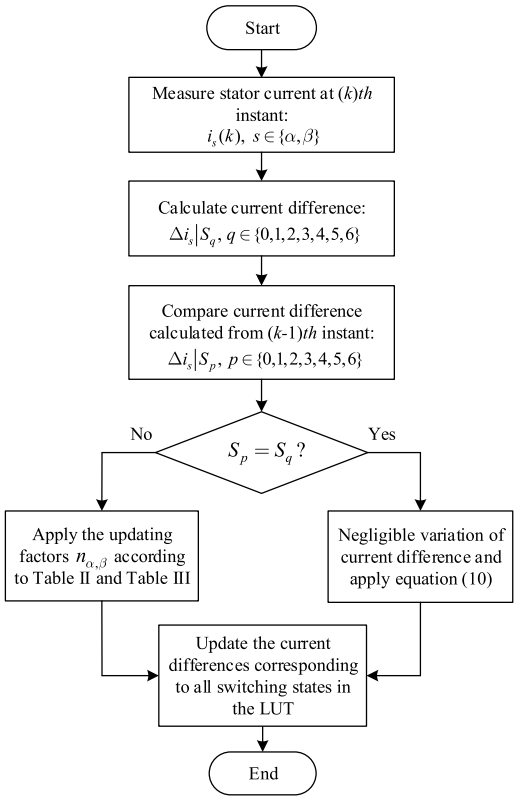

FIGURE 4. Flowchart of the proposed synchronized current difference update.

difference and written as

$$\begin{cases} \Delta i_\alpha|\,S_{0,1,\cdots,6} = \int_0^{T_s} \dfrac{di_\alpha}{dt}\Big|\,S_{0,1,\cdots,6} \\ \Delta i_\beta|\,S_{0,1,\cdots,6} = \int_0^{T_s} \dfrac{di_\beta}{dt}\Big|\,S_{0,1,\cdots,6}. \end{cases} \tag{17}$$

By the same token, the natural response of the zero voltage vectors can be expressed as follows

$$\begin{cases} \Delta i_\alpha|\,S_0 = \delta i_\alpha|\,S_0 \\ \Delta i_\beta|\,S_0 = \delta i_\beta|\,S_0. \end{cases} \tag{18}$$

It is observed that the last two terms of (13) are precisely the same as that of (16). This suggests that the differential stator currents of active switching states (S_1, S_2, S_3, S_4, S_5, and S_6) contains both the components of the natural response and the enforced response. Given (17), one may rewrite (13) as

$$\begin{cases} \Delta i_\alpha|\,S_5 = \underbrace{-\delta i_\alpha}_{\text{enforced response}} + \underbrace{\delta i_\alpha|\,S_0}_{\text{natural response}} \\ \Delta i_\beta|\,S_5 = \underbrace{-\delta i_\beta}_{\text{enforced response}} + \underbrace{\delta i_\beta|\,S_0}_{\text{natural response}} \end{cases} \tag{19}$$

The corresponding current differences of other active switching states can be defined likewise as follows:

$$\begin{cases} \Delta i_\alpha|\,S_1 = 2\delta i_\alpha + \delta i_\alpha|\,S_0 \\ \Delta i_\beta|\,S_1 = \delta i_\beta|\,S_0 \end{cases} \tag{20}$$

$$\begin{cases} \Delta i_\alpha|\,S_2 = \delta i_\alpha + \delta i_\alpha|\,S_0 \\ \Delta i_\beta|\,S_2 = \delta i_\beta + \delta i_\beta|\,S_0 \end{cases} \tag{21}$$

$$\begin{cases} \Delta i_\alpha|\,S_3 = -\delta i_\alpha + \delta i_\alpha|\,S_0 \\ \Delta i_\beta|\,S_3 = \delta i_\beta + \delta i_\beta|\,S_0 \end{cases} \tag{22}$$

$$\begin{cases} \Delta i_\alpha|\,S_4 = -2\delta i_\alpha + \delta i_\alpha|\,S_0 \\ \Delta i_\beta|\,S_4 = \delta i_\beta|\,S_0 \end{cases} \tag{23}$$

$$\begin{cases} \Delta i_\alpha|\,S_6 = \delta i_\alpha + \delta i_\alpha|\,S_0 \\ \Delta i_\beta|\,S_6 = -\delta i_\beta + \delta i_\beta|\,S_0 \end{cases} \tag{24}$$

where δi_α and δi_β are the $\alpha\beta$ enforced response of the stator current in the active switching states defined as

$$\begin{cases} \delta i_\alpha = \int_0^{T_s} \dfrac{2V_{dc}}{3\,(2L_{ls}+3L_s)}dt \\ \delta i_\beta = \int_0^{T_s} \dfrac{2\sqrt{3}\,V_{dc}}{3\,(2L_{ls}+3L_s)}dt. \end{cases} \tag{25}$$

B. THE TABLE OF CURRENT DIFFERENCE UPDATE

Suppose that S_p is first the applied switching state followed by S_q. Following equations (18) to (24), one may get

$$\begin{cases} \Delta i_\alpha|\,S_p = \delta i_\alpha + \delta i_\alpha|\,S_0 \\ \Delta i_\beta|\,S_p = \delta i_\beta + \delta i_\beta|\,S_0 \end{cases} \tag{26}$$

Likewise, the succeeding switching state S_q can be obtained as

$$\begin{cases} \Delta i_\alpha|\,S_q = \delta i_\alpha + \delta i_\alpha|\,S_0 \\ \Delta i_\beta|\,S_q = \delta i_\beta + \delta i_\beta|\,S_0 \end{cases} \tag{27}$$

where $S_p, S_q \in \{S_0, S_1, S_2, S_3, S_4, S_5, S_6\}$ represents any two of the switching states, with p being different from $q (p \neq q)$.

$$A = \begin{bmatrix} \dfrac{2}{3\,(2L_{ls}+3L_s)} \\ \dfrac{2}{\sqrt{3}\,(2L_{ls}+3L_s)} \end{bmatrix} \tag{14}$$

$$\begin{bmatrix} \lambda_\alpha \\ \lambda_\beta \end{bmatrix} = \lambda_m \begin{bmatrix} \dfrac{-d\left(\cos\left(\dfrac{2\pi}{3}-\theta_e\right)\right) + 2d\,(\cos(\theta_e)) - d\left(\cos\left(\dfrac{2\pi}{3}+\theta_e\right)\right)}{dt} \\ \dfrac{2d\left(\cos\left(\dfrac{2\pi}{3}-\theta_e\right)\right) - d\left(\cos\left(\dfrac{2\pi}{3}+\theta_e\right)\right)}{dt} \end{bmatrix} \tag{15}$$

TABLE 2. The update factor n_α for α-axis current difference.

S_p / S_q	S_0	S_1	S_2	S_3	S_4	S_5	S_6
S_0		-2	-1	1	2	1	-1
S_1	2		1	3	4	3	1
S_2	1	-1		2	3	2	0
S_3	-1	-3	-2		1	0	-2
S_4	-2	-4	-3	-1		-1	-3
S_5	-1	-3	-2	0	1		-2
S_6	1	-1	0	2	3	2	

TABLE 3. The update factor n_β for β-axis current difference.

S_p / S_q	S_0	S_1	S_2	S_3	S_4	S_5	S_6
S_0		0	-1	-1	0	1	1
S_1	0		-1	-1	0	1	1
S_2	1	1		0	1	2	2
S_3	1	1	0		1	2	2
S_4	0	0	-1	-1		1	1
S_5	-1	-1	-2	-2	-1		0
S_6	-1	-1	-2	-2	-1	0	

The correlation between current differences can be summarized by the updating tables – Tables 2 and 3. Their entities are obtained from the current slopes between two switching states applied in succession whose definitions are as follows:

$$\begin{cases} \Delta i_\alpha \big| S_q - \Delta i_\alpha \big| S_p = n_\alpha * \delta i_\alpha \\ \Delta i_\beta \big| S_q - \Delta i_\beta \big| S_p = n_\beta * \delta i_\beta \end{cases} \tag{28}$$

where variables n_α and n_β denote the updating factors. The above implies that the current difference is substantially affected by the dc-link voltage. To correct and update deviations in the enforced response, updating factors are introduced to the proposed SCDU-MFPCC. The updating technique is implemented on the stored current difference listed in the LUT.

Consider the current difference relationship between the selected switching states S_0 and S_5 as an example. The current differences are represented by $\Delta i_{\alpha,\beta} \big| S_0$ and $\Delta i_{\alpha,\beta} \big| S_5$. See Appendices A and B for detailed calculations of the two switching states. Suppose the previously applied switching state is S_5 followed by the switching state S_0, the variation of the current differences can be expressed as $\Delta i_{\alpha,\beta} \big| S_0 - \Delta i_{\alpha,\beta} \big| S_5$. By inspecting Tables 2 and 3, one gets the current slope as 1. As such, updating factors $n_\alpha = 1$ and $n_\beta = 1$ will be applied to correct the enforced response $\delta i_{\alpha,\beta}$. If the application sequence is reversed, such that $\Delta i_{\alpha,\beta} \big| S_5 - \Delta i_{\alpha,\beta} \big| S_0$, then $n_\alpha = -1$ and $n_\beta = -1$ are obtained as updating factors.

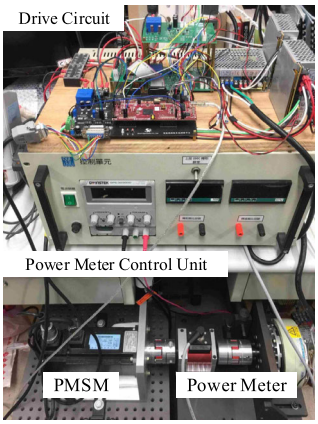

FIGURE 5. Experimental platform.

C. PRINCIPLE OF SCDU-MFPCC

The current prediction (9) is employed by the proposed SCDU-MFPCC. However, to improve the updating technique, an updating factor is introduced as depicted by (28). Equation (26) can be compactly written as $\Delta i_{\alpha,\beta} \big| S_{k-1} = \Delta i_{\alpha,\beta} \big| S_p$, and the same rule applied to (27) as $\Delta i_{\alpha,\beta} \big| S_k = \Delta i_{\alpha,\beta} \big| S_q$ in the next sampling period. The relationship of any two successive switching states, S_p and S_q, plays a significant role in performing the proposed synchronized current difference update. As seen in Tables 2 and 3, the update can be performed in two different ways depending on which switching states are applied. The following are defined accordingly:

1) If two successive switching states are different or distinct from each other, the factors $n_{\alpha,\beta}$ are applied to update their current difference.
2) If two successive switching states are alike, their current difference is assumed negligible, and (10) is implemented.

In this case, no matter which switching states are applied, real-time updates in the LUT can be guaranteed at any moment. With the proposed synchronized update, the frequent problem in the conventional MFPCC of stagnation in the stored current difference can effectively address. The flowchart in Fig. 4 further illustrates the update mechanism of the proposed SCDU-MFPCC.

V. EXPERIMENTAL VALIDATION

Shown in Fig. 5 is a prototype experimental platform to assess the performance of the proposed SCDU-MFPCC. The test bench consists of a drive circuit, a power control, a PMSM, and a power meter. A 32-bit floating-point dual-core TMS320F28379D microcontroller of Texas Instruments is utilized for real-time implementation. The drive circuit board comprises some key components, including two current sensors (LEM LA25-NP) and A/D conversion circuits (AD4001 and ADA4940). Specifications of the PMSM are given in Table 4, and the sampling period is set to be 100μs. Performance comparisons of the SCDU-MFPCC against the conventional MFPCC [23] are made.

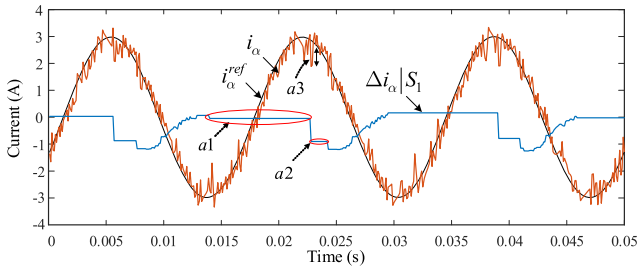

FIGURE 6. The stagnation effect under switching state S_1.

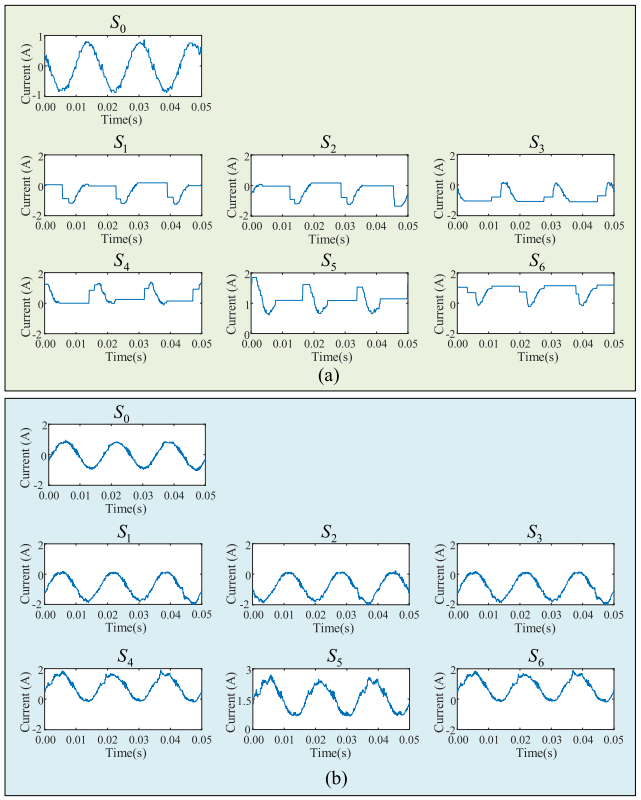

FIGURE 7. The current difference waveforms under different switching states at 900 rpm and 4 Nm load torque: (a) conventional MFPCC [23] and (b) proposed SCDU-MFPCC.

A. EFFECT OF CURRENT DIFFERENCE STAGNATION

Figure 6 shows the experimental waveform of the α-phase current. As can be observed, the current difference contains a steady horizontal line segment, indicating stagnation in the stored current difference. For analysis, let us consider the switching response of $\Delta i_\alpha | S_1$. The horizontal line implies that the switching state S_1 is either not selected or applied successively as the optimal switching mode during the period. The stored value in the LUT is unchanged with the current waveforms "$a1$". It can be noticed that the stagnation may seem to have a trivial effect on the current ripples. However, the stagnation can cause a sudden shifting in the current ripples between "$a1$" and "$a2$" during a relatively long period. As a result, a distorted signal is generated in "$a3''$ due to large current errors. It is therefore confirmed that prolonged stagnation in the LUT can result in undesirable predictions.

TABLE 4. PMSM specifications.

Parameter	Unit	Value
Rated Power	W	1000
Rated Speed	rpm	2000
Rated Torque	Nm	4.8
Number of Poles	pair	4
Stator Resistance	Ω	1.57
d-axis inductance	mH	5.1
q-axis inductance	mH	5.1

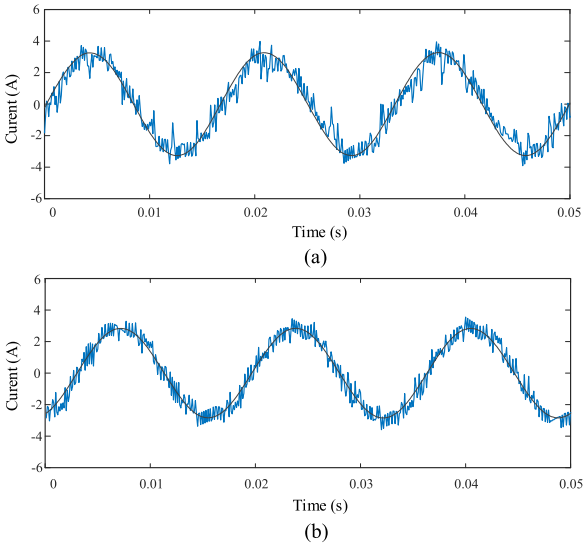

FIGURE 8. The α current response at 900 rpm and 4 Nm load torque: (a) conventional MFPCC [23] and (b) proposed SCDU-MFPCC.

B. ANTI-STAGNATION PERFORMANCE

The two controllers are tested under the same speed command of 900 rpm and the same disturbance load torque of 4 Nm.

Illustrated in Fig. 7 are the waveforms of current difference under the seven switching states (S_0 to S_6). For conventional MFPCC, active switching states are characterized by numerous horizontal line segments due to the stagnation effect. Under the same operating conditions, the proposed SCDU-MFPCC in Fig. 7(b) exhibits a standard sinusoidal waveform in all switching states, which reveals at any instant, their current differences are corrected and updated in the LUT according to the updating factors $n_{\alpha,\beta}$. It is also worth noting that the zero switching state S_0 on both controllers yields the same sinusoidal waveform as a result of the so-called natural response. This finding is consistent with Appendix B, where the differential stator currents of the zero voltage vectors are defined by the components of stator currents and the speed of the motor load [25].

The waveform of the α-phase current of the conventional MFPCC and the proposed SCDU-MFPCC is shown in Fig. 8. As can be seen, the current waveform of the proposed SCDU-MFPCC exhibits lesser fluctuations, particularly on the amplitudes. The current ripples are distinguishably more uniformed than that of the conventional MFPCC, as shown in Fig. 8(a). Quantitatively, the performance indices

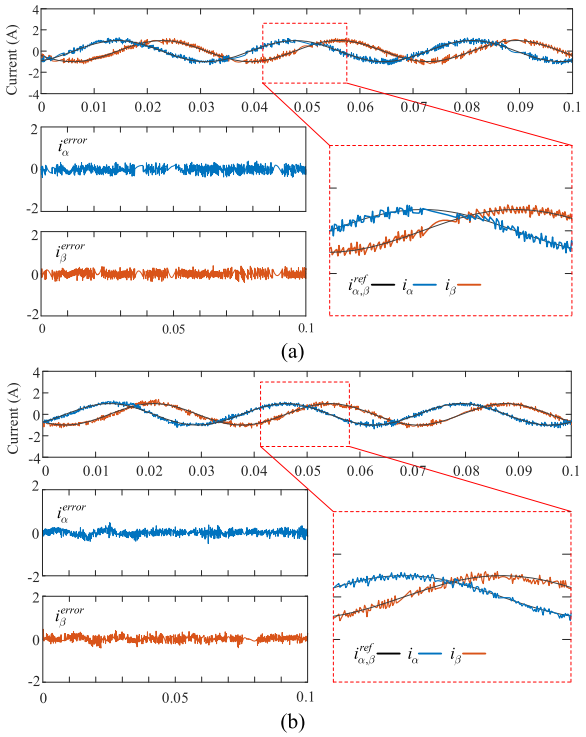

FIGURE 9. Steady-state current response under current command 1A and frequency 30 Hz, (a) conventional MFPCC [23] and (b) proposed SCDU-MFPCC. In the lower left figures: the α-phase and β-phase current prediction errors.

TABLE 5. Performance indices based on Fig. 8.

Methods	Average Current Error (A)	Average Current Ripple (A)	THD (%)
Conventional MFPCC	0.51	0.66	6.87
Proposed SCDU-MFPCC	0.40	0.48	3.73

of average current error, average current ripple, and total harmonic distortion (THD) are calculated and given in Table 5.

C. ASSESSMENT OF STEADY-STATE PERFORMANCE

Two tests of current and speed command are performed to assess the flexibility of the controllers in various conditions. Under current commands, the motor is operated at 1A and 6A, respectively, both with a frequency of 30 Hz. Likewise, for the speed commands, 600 rpm and 1200 rpm are performed, respectively. The motor runs under a load torque of 2 Nm.

Fig. 9 shows the steady-state current response under 1A and a frequency of 30 Hz. It can be seen from their current waveforms that both schemes yield minimum current ripples and spikes. However, compared to its counterpart, the proposed SCDU-MFPCC has less current oscillations while tracking the reference. In contrast, it can be seen in the enlarged section of Fig. 9(a) for the conventional MFPCC that substantial stagnation is observed where sudden shifting of the current waveform is present. The same observations can be noticed under a higher current command of 6A in

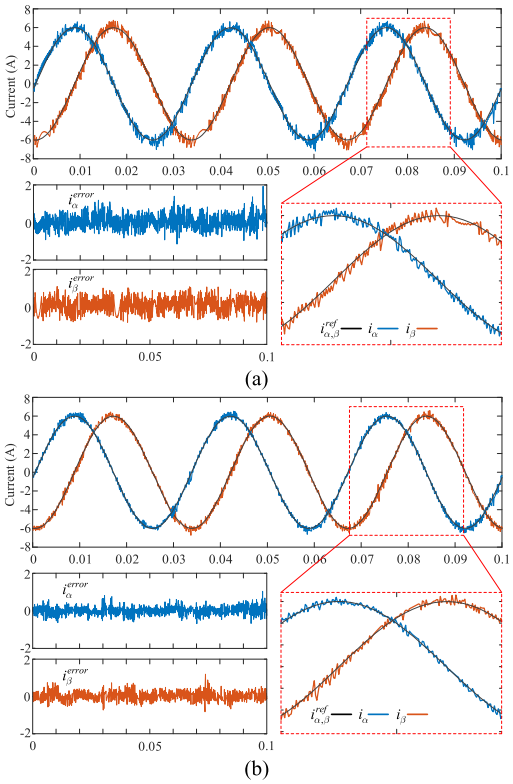

FIGURE 10. Steady-state current response under current command 6A and frequency 30 Hz, (a) conventional MFPCC [23] and (b) proposed SCDU-MFPCC. In the lower left figures: the α-phase and β-phase current prediction errors.

Fig. 10. Apparently, the proposed SCDU-MFPCC is substantially outperformed the conventional MFPCC with much better tracking accuracy and lesser current ripples in that the current errors in Figs. 9 and 10 are reduced significantly.

Illustrated in Fig. 11 and 12 are the waveforms of stator currents under constant low-speed and high-speed commands and a load-torque of 2 Nm. The $\alpha\beta$ current prediction errors are evidently enhanced than the conventional MFPCC in Fig. 11(a). The current response of the proposed SCDU-MFPCC showed in Fig. 11(b) exhibits better and smoother tracking performance. The current ripples are considerably reduced, owing to the updating scheme implemented in the proposed method. In the case of higher speed command at 1200 rpm in Fig. 12, the proposed scheme is seen to eliminate heavy and large current ripples that are visible in the conventional MFPCC. The tracking accuracy is better and more stable. In short, the experimental results demonstrate that the proposed SCDU-MFPCC can effectively suppress the effect of current difference stagnation and achieved better steady-state performance.

D. ASSESSMENT OF DYNAMIC PERFORMANCE

A series of experiments are conducted to evaluate the performance of the proposed method under dynamic settings. Four different tests are performed, including the current step command in Fig. 13 and 14, a progressively varying load-torque in Fig. 15, and a speed step command in Fig. 16.

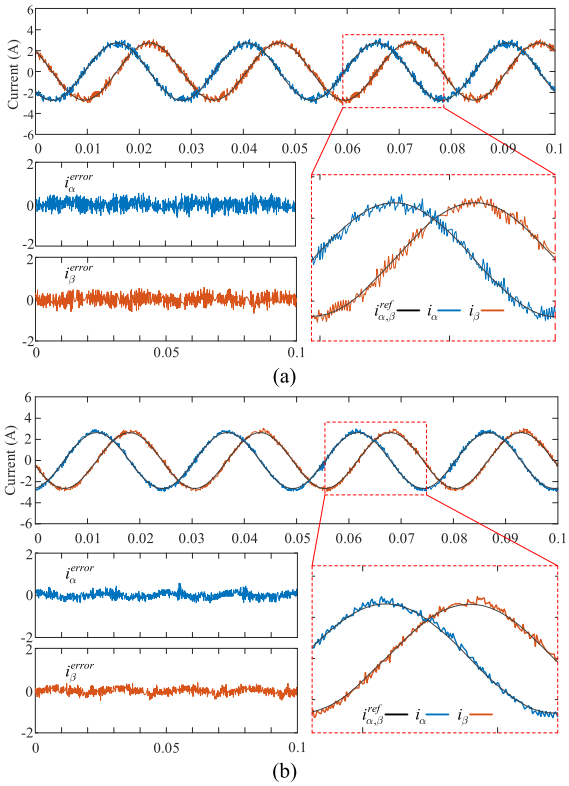

FIGURE 11. Steady-state current response under speed command 600 rpm and load-torque 2 Nm, (a) conventional MFPCC [23] and (b) proposed SCDU-MFPCC. In the lower left figures: the α-phase and β-phase current prediction errors.

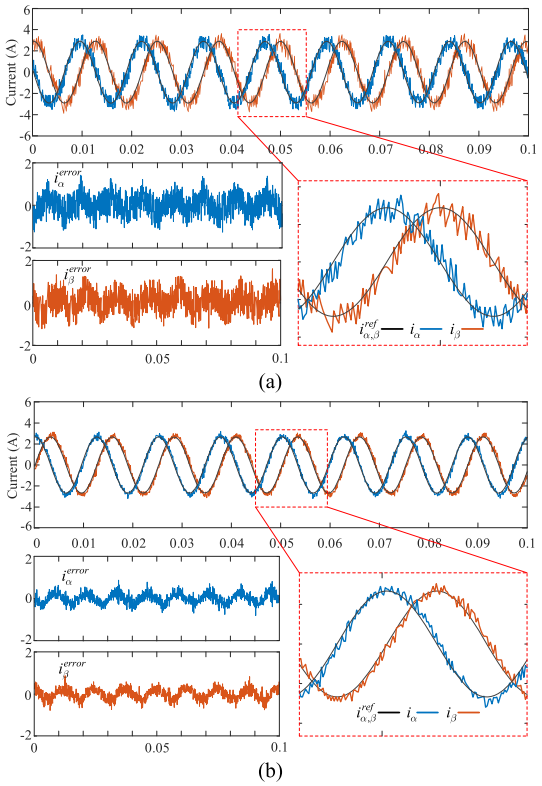

FIGURE 12. Steady-state current response under speed command 1200 rpm and load-torque 2 Nm, (a) conventional MFPCC [23] and (b) proposed SCDU-MFPCC. In the lower left figures: the α-phase and β-phase current prediction errors.

As shown in Fig. 13 is the current response from a current command jumping from 1A to 4A at 0.1 sec. It can be seen from the waveforms that both controllers exhibit a fast response from the abrupt command change. However, their waveforms in the enlarged sections reveal that the α-phase transient response of the conventional MFPCC shows distorted spikes and ripples. In contrast, the tracking performance of the proposed SCDU-MFPCC is much better, and only minor prediction errors are observed. Another result shown in Fig. 14 is the dynamic response of a current step command from -6A to 6A. Here, the α-phase current is expected to shift from the abrupt change of current amplitudes. As can be clearly seen from the response, the proposed method demonstrates excellent dynamic performance and lesser oscillations in the current ripples. Although the conventional method has a dynamic response with uniformed ripples, the impact from stagnation is still clearly evident.

Running at a constant speed of 300 rpm, Fig. 15 presents the current response under a progressively varying load-torque from 0.2 Nm to 2 Nm. The two controllers display quick responses from the sudden change of load-torque. However, the presence of heavy ripples and current spikes are more noticeable in the conventional MFPCC. The speed tracking performance is also illustrated in the figures, in which the proposed SCDU-MFPCC is observed to have a faster settling time than the conventional method. As a result, the error is reduced and significantly improved.

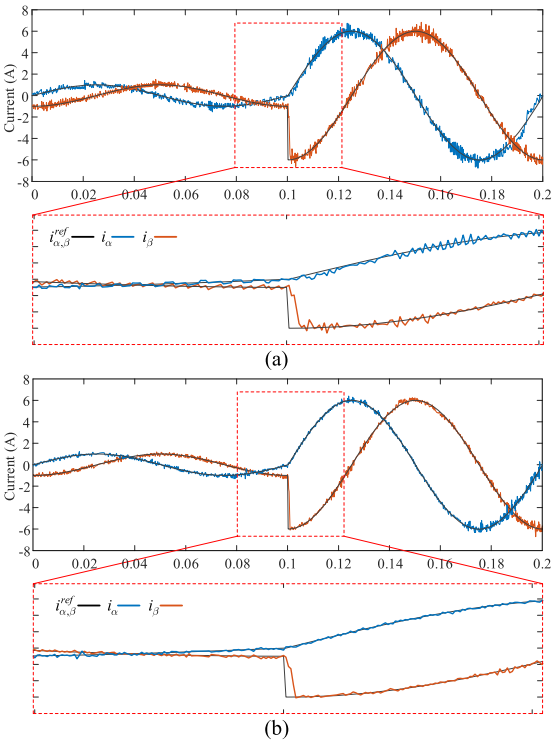

FIGURE 13. Dynamic current response under step current command from 1A to 4A, (a) conventional MFPCC [23] and (b) proposed SCDU-MFPCC.

The starting response from a standstill condition to a constant command speed of 2000 rpm is presented in Fig. 16.

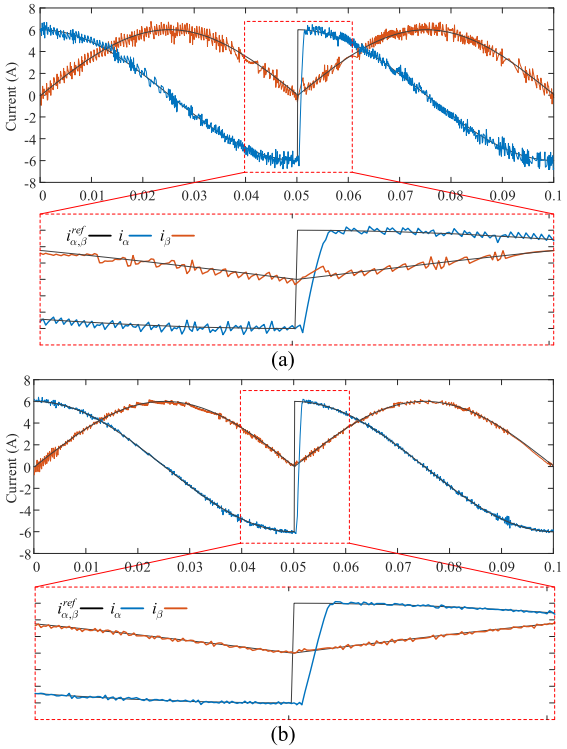

FIGURE 14. Dynamic current response under step current command in the α-phase from -6A to 6A, (a) conventional MFPCC [23] and (b) proposed SCDU-MFPCC.

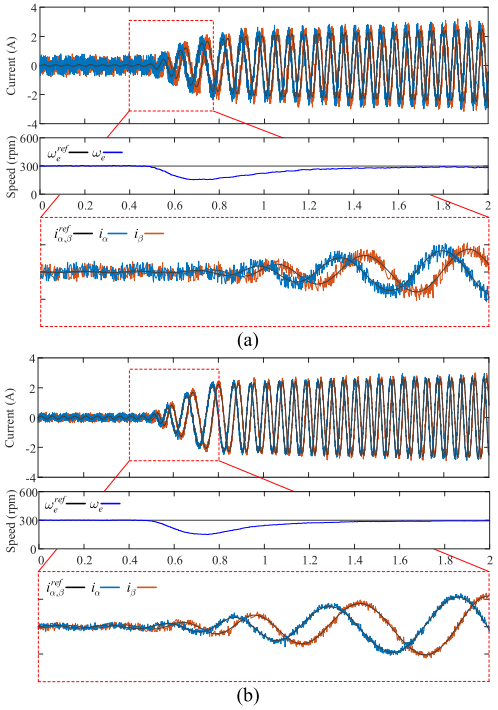

FIGURE 15. Dynamc current response under varying load-torque from 0.2 Nm to 2 Nm and constant speed 300 rpm, (a) conventional MFPCC [23] and (b) proposed SCDU-MFPCC. In the middle figure: the speed response.

It can be seen that the dynamic response of the proposed SCDU-MFPCC is far better than the conventional method. The current response in Fig. 16(b) is substantially improved with lesser prediction errors and better harmonic distortions.

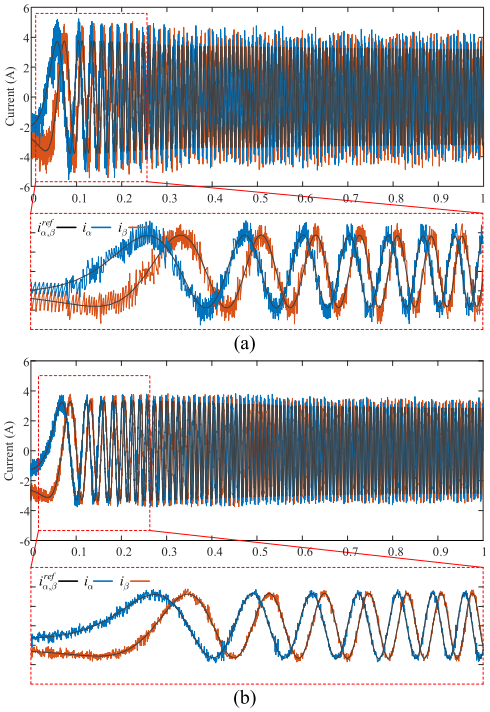

FIGURE 16. Dynamic current response from standstill condition (zero rpm) to maximum speed 2000 rpm, (a) conventional MFPCC [23] and (b) proposed SCDU-MFPCC.

Given the different experimental results presented, the proposed SCDU-MFPCC substantially eliminates the undesirable stagnation. The dynamic response is faster and better than that of the conventional MFPCC.

VI. CONCLUSION

This paper presents a novel method that features a novel current difference update to improve conventional methods. Specifically, the work proposes a synchronized current difference update for model-free predictive current control (SCDU-MFPCC). Unlike conventional MFPCCs, the proposed method makes use of updating factors to correct the response of voltage vectors. These updating factors are obtained from the current slope of the latest two applied switching states. The stored current difference can be renewed simultaneously, hence the entire LUT can be updated within every sampling period. Compared to the conventional MFPCCs, the proposed scheme substantially reduced the stagnation effect and yielded better steady-state and dynamic performances, which were demonstrated and verified by experimental results presented in the paper.

APPENDIX A

This section contains the detailed analysis and derivation of updating factor n of selected switching states. Variables used are defined previously. Let us consider the circuit diagram of $S_5(001)$ shown in Fig. 3. The following equations can be derived *via* KVL:

$$V_{dc} = v_c - v_a \tag{A1}$$

$$v_a = v_b \tag{A2}$$

It can be recalled that the stator voltage equation of PMSM is given as

$$\begin{bmatrix} v_a \\ v_b \\ v_c \end{bmatrix} = \begin{bmatrix} R_s & 0 & 0 \\ 0 & R_s & 0 \\ 0 & 0 & R_s \end{bmatrix} \begin{bmatrix} i_a \\ i_b \\ i_c \end{bmatrix} + \begin{bmatrix} L_{aa} & L_{ab} & L_{ac} \\ L_{ba} & L_{bb} & L_{bc} \\ L_{ca} & L_{cb} & L_{cc} \end{bmatrix} \begin{bmatrix} \frac{di_a}{dt} \\ \frac{di_b}{dt} \\ \frac{di_c}{dt} \end{bmatrix} + \frac{d}{dt} \begin{bmatrix} \lambda_m \cos\theta_e \\ \lambda_m \cos\left(\theta_e - \frac{2}{3}\pi\right) \\ \lambda_m \cos\left(\theta_e + \frac{2}{3}\pi\right) \end{bmatrix} \tag{A3}$$

Substituting the corresponding values of (A3) to (A1) and (A2) can yield the following equations:

$$\begin{aligned} V_{dc} &= R_s i_c + \left(L_{ca}\frac{di_a}{dt} + L_{cb}\frac{di_b}{dt} + L_{cc}\frac{di_c}{dt}\right) \\ &\quad + \frac{d}{dt}\left(\lambda_m \cos\left(\theta_e + \frac{2}{3}\pi\right)\right) \\ &\quad - \left\{R_s i_a + \left(L_{aa}\frac{di_a}{dt} + L_{ab}\frac{di_b}{dt} + L_{ac}\frac{di_c}{dt}\right) \right. \\ &\quad \left. + \frac{d}{dt}\left(\lambda_m \cos\left(\theta_e\right)\right)\right\} \end{aligned} \tag{A4}$$

$$\begin{aligned} &R_s i_a + \frac{d}{dt}\left(L_{aa}\frac{di_a}{dt} + L_{ab}\frac{di_b}{dt} + L_{ac}\frac{di_c}{dt}\right) \\ &\quad + \frac{d}{dt}\left(\lambda_m \cos\left(\theta_e\right)\right) \\ &= R_s i_b + \left(L_{ba}\frac{di_a}{dt} + L_{bb}\frac{di_b}{dt} + L_{bc}\frac{di_c}{dt}\right) \\ &\quad + \frac{d}{dt}\left(\lambda_m \cos\left(\theta_e - \frac{2}{3}\pi\right)\right) \end{aligned} \tag{A5}$$

Simplifying (A4) and (A5) into matrix form becomes

$$\begin{bmatrix} V_{dc} \\ 0 \\ 0 \end{bmatrix} = \begin{bmatrix} -R_s & 0 & R_s \\ R_s & -R_s & 0 \\ 0 & 0 & 0 \end{bmatrix} \begin{bmatrix} i_a \\ i_b \\ i_c \end{bmatrix} + A \begin{bmatrix} \frac{di_a}{dt} \\ \frac{di_b}{dt} \\ \frac{di_c}{dt} \end{bmatrix}, + \begin{bmatrix} \frac{d}{dt}\left(\lambda_m \cos\left(\theta_e + \frac{2}{3}\pi\right)\right) - \frac{d}{dt}(\lambda_m \cos\theta_e) \\ \frac{d}{dt}\left(\lambda_m \cos\left(\theta_e\right)\right) - \frac{d}{dt}\left(\lambda_m \cos\left(\theta_e - \frac{2}{3}\pi\right)\right) \\ 0 \end{bmatrix} \tag{A6}$$

where

$$A = \begin{bmatrix} L_{ca} - L_{aa} & L_{cb} - L_{ab} & L_{cc} - L_{ac} \\ L_{aa} - L_{ba} & L_{ab} - L_{bb} & L_{ac} - L_{bc} \\ 1 & 1 & 1 \end{bmatrix}.$$

From (A6), the differential stator current of $S_5(001)$ can be obtained in the expression of

$$\begin{aligned} &\left[\begin{array}{c|c} \frac{di_a}{dt} & S_5 \\ \frac{di_b}{dt} & S_5 \\ \frac{di_c}{dt} & S_5 \end{array}\right] \\ &= A^{-1}\begin{bmatrix} V_{dc} \\ 0 \\ 0 \end{bmatrix} \\ &\quad - A^{-1}\begin{bmatrix} -R_s & 0 & R_s \\ R_s & -R_s & 0 \\ 0 & 0 & 0 \end{bmatrix}\begin{bmatrix} i_a \\ i_b \\ i_c \end{bmatrix} \\ &\quad - A^{-1}\begin{bmatrix} \frac{d}{dt}\left(\lambda_m \cos\left(\theta_e + \frac{2}{3}\pi\right)\right) - \frac{d}{dt}(\lambda_m \cos\theta_e) \\ \frac{d}{dt}\left(\lambda_m \cos\left(\theta_e\right)\right) - \frac{d}{dt}\left(\lambda_m \cos\left(\theta_e - \frac{2}{3}\pi\right)\right) \\ 0 \end{bmatrix}. \end{aligned} \tag{A7}$$

The three-phase coil winding of the PMSM is characterized by an equal self-inductance and mutual inductance. Hence, the following conditions can be considered:

$$\begin{cases} L_{aa} = L_{bb} = L_{cc} = L_s + L_{ls} \\ L_{ab} = L_{ac} = L_{ba} = L_{bc} \\ = \ldots\ldots = L_{ca} = L_{cb} = L_s \cos\left(\frac{2\pi}{3}\right) = -\frac{1}{2}L_s. \end{cases} \tag{A8}$$

Therefore (A7) can be simplified into (A9), as shown at the top of the next page.

Then, converting the given equation in $\alpha\beta$ reference coordinates will deduce the following equation (A10), as shown at the top of the next page.

APPENDIX B

From Fig. 5, the zero switching state (000) or (111) can yield the following equations:

$$v_a = v_b \tag{B1}$$

$$v_a = v_c. \tag{B2}$$

Substituting the corresponding values of (A3) to (B1) and (B2) will result in the following equations:

$$\begin{aligned} &R_s i_a + \frac{d}{dt}\left(L_{aa}\frac{di_a}{dt} + L_{ab}\frac{di_b}{dt} + L_{ac}\frac{di_c}{dt}\right) + \frac{d}{dt}\left(\lambda_m \cos\left(\theta_e\right)\right) \\ &= R_s i_b + \left(L_{ba}\frac{di_a}{dt} + L_{bb}\frac{di_b}{dt} + L_{bc}\frac{di_c}{dt}\right) \\ &\quad + \frac{d}{dt}\left(\lambda_m \cos\left(\theta_e - \frac{2}{3}\pi\right)\right) \end{aligned} \tag{B3}$$

$$\begin{aligned} &R_s i_a + \left(L_{aa}\frac{di_a}{dt} + L_{ab}\frac{di_b}{dt} + L_{ac}\frac{di_c}{dt}\right) + \frac{d}{dt}\left(\lambda_m \cos\left(\theta_e\right)\right) \\ &= R_s i_c + \left(L_{ca}\frac{di_a}{dt} + L_{cb}\frac{di_b}{dt} + L_{cc}\frac{di_c}{dt}\right) \end{aligned}$$

$$\begin{bmatrix} \frac{di_a}{dt}\Big|S_5 \\ \frac{di_b}{dt}\Big|S_5 \\ \frac{di_c}{dt}\Big|S_5 \end{bmatrix} = \begin{bmatrix} -\frac{2V_{dc}}{9L_s+6L_{ls}} \\ -\frac{2V_{dc}}{9L_s+6L_{ls}} \\ \frac{4V_{dc}}{9L_s+6L_{ls}} \end{bmatrix} + \begin{bmatrix} \frac{2(2i_a-i_b-i_c)R_s}{9L_s+6L_{ls}} \\ -\frac{2(i_a-2i_b+i_c)R_s}{9L_s+6L_{ls}} \\ -\frac{2(i_a+i_b-2i_c)R_s}{9L_s+6L_{ls}} \end{bmatrix} + \begin{bmatrix} \frac{2\left(-d\cos\left(\frac{2\pi}{3}-\theta_e\right)+2d\cos(\theta_e)-d\cos\left(\frac{2\pi}{3}+\theta_e\right)\right)\lambda_m}{3(3L_s+2L_{ls})\,dt} \\ \frac{2\left(2d\cos\left(\frac{2\pi}{3}-\theta_e\right)-d\cos(\theta_e)-d\cos\left(\frac{2\pi}{3}+\theta_e\right)\right)\lambda_m}{3(3L_s+2L_{ls})\,dt} \\ \frac{2\left(-d\cos\left(\frac{2\pi}{3}-\theta_e\right)-d\cos[\theta_e]+2d\cos\left(\frac{2\pi}{3}+\theta_e\right)\right)\lambda_m}{3(3L_s+2L_{ls})\,dt} \end{bmatrix}. \quad \text{(A9)}$$

$$\begin{bmatrix} \frac{di_\alpha}{dt}\Big|S_5 \\ \frac{di_\beta}{dt}\Big|S_5 \end{bmatrix} = \begin{bmatrix} -\frac{2V_{dc}}{3(3L_s+2L_{ls})} \\ -\frac{2V_{dc}}{\sqrt{3}(3L_s+2L_{ls})} \end{bmatrix} + \begin{bmatrix} \frac{2(2i_a-i_b-i_c)R_s}{3(3L_s+2L_{ls})} \\ \frac{2(i_b-i_c)R_s}{\sqrt{3}(3L_s+2L_{ls})} \end{bmatrix} + \begin{bmatrix} \frac{2\left(-d\cos\left(\frac{2\pi}{3}-\theta_e\right)+2d\cos(\theta_e)-d\cos\left(\frac{2\pi}{3}+\theta_e\right)\right)\lambda_m}{3(3L_s+2L_{ls})\,dt} \\ \frac{2\left(d\cos\left(\frac{2\pi}{3}-\theta_e\right)-d\cos\left(\frac{2\pi}{3}+\theta_e\right)\right)\lambda_m}{\sqrt{3}(3L_s+2L_{ls})\,dt} \end{bmatrix}. \quad \text{(A10)}$$

$$\begin{bmatrix} \frac{di_\alpha}{dt}\Big|S_0 \\ \frac{di_\beta}{dt}\Big|S_0 \end{bmatrix} = \begin{bmatrix} \frac{2(2i_a-i_b-i_c)R_s}{3(3L_s+2L_{ls})} \\ \frac{2(i_b-i_c)R_s}{\sqrt{3}(3L_s+2L_{ls})} \end{bmatrix} + \begin{bmatrix} \frac{2\left(-d\cos\left(\frac{2\pi}{3}-\theta_e\right)+2d\cos(\theta_e)-d\cos\left(\frac{2\pi}{3}+\theta_e\right)\right)\lambda_m}{3(3L_s+2L_{ls})\,dt} \\ \frac{2\left(d\cos\left(\frac{2\pi}{3}-\theta_e\right)-d\cos\left(\frac{2\pi}{3}+\theta_e\right)\right)\lambda_m}{\sqrt{3}(3L_s+2L_{ls})\,dt} \end{bmatrix}. \quad \text{(B5)}$$

$$+\frac{d}{dt}\left(\lambda_m\cos\left(\theta_e+\frac{2}{3}\pi\right)\right). \quad \text{(B4)}$$

Following the same procedures from (A6) to (A10), the differential stator current of $S_1(000)/(111)$ in $\alpha\beta$ reference is given as (B5), shown at the top of the page.

REFERENCES

[1] S. Yamamoto, H. Hirahara, A. Tanaka, T. Ara, and K. Matsuse, "Universal sensorless vector control of induction and permanent-magnet synchronous motors considering equivalent iron loss resistance," *IEEE Trans. Ind. Appl.*, vol. 51, no. 2, pp. 1259–1267, Mar./Apr. 2015, doi: 10.1109/TIA.2014.2360962.

[2] D. Basic, F. Malrait, and P. Rouchon, "Current controller for low-frequency signal injection and rotor flux position tracking at low speeds," *IEEE Trans. Ind. Electron.*, vol. 58, no. 9, pp. 4010–4022, Sep. 2011, doi: 10.1109/TIE.2010.2100336.

[3] B. Wang, C. Zhang, Q. Jia, X. Liu, and G. Yang, "Robust continuous sliding mode control for manipulator PMSM trajectory tracking system under time-varying uncertain disturbances," *IEEE Access*, vol. 8, pp. 196618–196632, 2020, doi: 10.1109/ACCESS.2020.3034220.

[4] X. Lin, W. Huang, W. Jiang, Y. Zhao, D. Dong, and X. Wu, "Direct torque control for three-phase open-end winding PMSM with common DC bus based on duty ratio modulation," *IEEE Trans. Power Electron.*, vol. 35, no. 4, pp. 4216–4232, Apr. 2020, doi: 10.1109/TPEL.2019.2935295.

[5] Z. Tang and B. Akin, "A new LMS algorithm based deadtime compensation method for PMSM FOC drives," *IEEE Trans. Ind. Appl.*, vol. 54, no. 6, pp. 6472–6484, Nov./Dec. 2018, doi: 10.1109/TIA.2018.2853045.

[6] K. Liu, C. Hou, and W. Hua, "A novel inertia identification method and its application in PI controllers of PMSM drives," *IEEE Access*, vol. 7, pp. 13445–13454, 2019, doi: 10.1109/ACCESS.2019.2894342.

[7] V. Yaramasu and B. Wu, "Fundamentals of model predictive control," in *Model Predictive Control of Wind Energy Conversion Systems*. Hoboken, NJ, USA: Wiley, 2017, pp. 117–148, doi: 10.1002/9781119082989.ch4.

[8] F. Wang, K. Zuo, P. Tao, and J. Rodríguez, "High performance model predictive control for PMSM by using stator current mathematical model self-regulation technique," *IEEE Trans. Power Electron.*, vol. 35, no. 12, pp. 13652–13662, Dec. 2020, doi: 10.1109/TPEL.2020.2994948.

[9] J. Chen and Y. Zhang, "Dual-vector model predictive current control of permanent magnet synchronous motor drives with the segment golden search method," *IEEE Access*, vol. 8, pp. 183826–183846, 2020, doi: 10.1109/ACCESS.2020.3026542.
[10] C.-S. Lim, E. Levi, M. Jones, N. A. Rahim, and W.-P. Hew, "A comparative study of synchronous current control schemes based on FCS-MPC and PI-PWM for a two-motor three-phase drive," *IEEE Trans. Ind. Electron.*, vol. 61, no. 8, pp. 3867–3878, Aug. 2014, doi: 10.1109/TIE.2013.2286573.
[11] A. A. Ahmed, B. K. Koh, and Y. I. Lee, "A comparison of finite control set and continuous control set model predictive control schemes for speed control of induction motors," *IEEE Trans. Ind. Informat.*, vol. 14, no. 4, pp. 1334–1346, Apr. 2018, doi: 10.1109/TII.2017.2758393.
[12] T. Li, R. Ma, and W. Han, "Virtual-vector-based model predictive current control of five-phase PMSM with stator current and concentrated disturbance observer," *IEEE Access*, vol. 8, pp. 212635–212646, 2020, doi: 10.1109/ACCESS.2020.3040558.
[13] T. Wang, Y. Hu, Z. Wu, and K. Ni, "Low-switching-loss finite control set model predictive current control for IMs considering rotor-related inductance mismatch," *IEEE Access*, vol. 8, pp. 108928–108941, 2020, doi: 10.1109/ACCESS.2020.3001767.
[14] O. Wallscheid and E. F. B. Ngoumtsa, "Investigation of disturbance observers for model predictive current control in electric drives," *IEEE Trans. Power Electron.*, vol. 35, no. 12, pp. 13563–13572, Dec. 2020, doi: 10.1109/TPEL.2020.2992784.
[15] H. A. Young, M. A. Perez, and J. Rodriguez, "Analysis of finite-control-set model predictive current control with model parameter mismatch in a three-phase inverter," *IEEE Trans. Ind. Electron.*, vol. 63, no. 5, pp. 3100–3107, May 2016, doi: 10.1109/TIE.2016.2515072.
[16] J. Rodríguez, R. Heydari, Z. Rafiee, H. A. Young, F. Flores-Bahamonde, and M. Shahparasti, "Model-free predictive current control of a voltage source inverter," *IEEE Access*, vol. 8, pp. 211104–211114, 2020, doi: 10.1109/ACCESS.2020.3039050.
[17] M. Bermudez, M. R. Arahal, M. J. Duran, and I. Gonzalez-Prieto, "Model predictive control of six-phase electric drives including ARX disturbance estimator," *IEEE Trans. Ind. Electron.*, vol. 68, no. 1, pp. 81–91, Jan. 2021, doi: 10.1109/TIE.2019.2962477.
[18] J. Ren, Y. Ye, G. Xu, Q. Zhao, and M. Zhu, "Uncertainty-and-disturbance-estimator-based current control scheme for PMSM drives with a simple parameter tuning algorithm," *IEEE Trans. Power Electron.*, vol. 32, no. 7, pp. 5712–5722, Jul. 2017, doi: 10.1109/TPEL.2016.2607228.
[19] J. Talla, V. Q. Leu, V. Šmídl, and Z. Peroutka, "Adaptive speed control of induction motor drive with inaccurate model," *IEEE Trans. Ind. Electron.*, vol. 65, no. 11, pp. 8532–8542, Nov. 2018, doi: 10.1109/TIE.2018.2811362.
[20] X. Zhang, L. Zhang, and Y. Zhang, "Model predictive current control for PMSM drives with parameter robustness improvement," *IEEE Trans. Power Electron.*, vol. 34, no. 2, pp. 1645–1657, Feb. 2019, doi: 10.1109/TPEL.2018.2835835.
[21] Y. Zhou, H. Li, R. Liu, and J. Mao, "Continuous voltage vector model-free predictive current control of surface mounted permanent magnet synchronous motor," *IEEE Trans. Energy Convers.*, vol. 34, no. 2, pp. 899–908, Jun. 2019, doi: 10.1109/TEC.2018.2867218.
[22] X. Yuan, S. Zhang, and C. Zhang, "Nonparametric predictive current control for PMSM," *IEEE Trans. Power Electron.*, vol. 35, no. 9, pp. 9332–9341, Sep. 2020, doi: 10.1109/TPEL.2020.2970173.
[23] C.-K. Lin, T.-H. Liu, J.-T. Yu, L.-C. Fu, and C.-F. Hsiao, "Model-free predictive current control for interior permanent-magnet synchronous motor drives based on current difference detection technique," *IEEE Trans. Ind. Electron.*, vol. 61, no. 2, pp. 667–681, Feb. 2014, doi: 10.1109/TIE.2013.2253065.
[24] C.-K. Lin, J.-T. Yu, Y.-S. Lai, and H.-C. Yu, "Improved model-free predictive current control for synchronous reluctance motor drives," *IEEE Trans. Ind. Electron.*, vol. 63, no. 6, pp. 3942–3953, Jun. 2016, doi: 10.1109/TIE.2016.2527629.
[25] P. G. Carlet, F. Tinazzi, S. Bolognani, and M. Zigliotto, "An effective model-free predictive current control for synchronous reluctance motor drives," *IEEE Trans. Ind. Appl.*, vol. 55, no. 4, pp. 3781–3790, Jul./Aug. 2019, doi: 10.1109/TIA.2019.2910494.
[26] P. Cortes, J. Rodriguez, C. Silva, and A. Flores, "Delay compensation in model predictive current control of a three-phase inverter," *IEEE Trans. Ind. Electron.*, vol. 59, no. 2, pp. 1323–1325, Feb. 2012, doi: 10.1109/TIE.2011.2157284.

CRESTIAN ALMAZAN AGUSTIN was born in Isabela, Philippines, in 1989. He received the B.S. degree in electrical engineering from Isabela State University, Ilagan, Philippines, in 2012, the M.S. degree in engineering management from the University of La Salette, Santiago, Philippines, in 2015, and the M.S. degree in electrical engineering from Saint Louis University, Cagayan, Philippines, in 2017. He is currently pursuing the Ph.D. degree in electrical engineering with National Taiwan Ocean University, Keelung, Taiwan. His research interests include control of motor drives and inverter topologies.

JEN-TE YU was born in Hualien, Taiwan. He received the M.S. degree in aerospace engineering from Wichita State University, USA, the M.S. degree in electrical engineering from the Georgia Institute of Technology, USA, and the Ph.D. degree in electrical engineering from National Taiwan University, Taiwan.

Since August 2016, he has been with the Department of Electrical Engineering, Chung Yuan Christian University (CYCU), Taiwan, as an Assistant Professor, where he currently serves as the Director of the Modern Control Laboratory. Prior to joining CYCU, he worked with the industry for years both in the U.S. and Taiwan, as an Engineer, and later as a Corporate Research and Development Manager. His current research interests include networked control subject to sporadic packet dropout, linear quadratic regulator theory, consensus of multiagent systems, and output feedback design of negative imaginary systems.

YU-SHAN CHENG (Member, IEEE) received the B.S. and Ph.D. degrees in electrical engineering from the National Taiwan University of Science and Technology, Taiwan, in 2012 and 2017, respectively. From 2015 to 2016, she stayed with the Technical University of Munich, Germany, as a Visiting Scholar. From 2017 to 2020, she works as a Project Researcher with Tokyo Metropolitan University, Japan. Since 2020, she has been a Faculty Member with the Department of Electrical Engineering, National Taiwan Ocean University. Her current research interests include power management of renewable energy systems, metaheuristic optimization, and power converters.

CHENG-KAI LIN was born in Taipei, Taiwan, in 1980. He received the B.S. degree in electrical engineering from the Ming Chi University of Technology, Taipei, Taiwan, in 2002, and the M.S. and Ph.D. degrees in electrical engineering from the National Taiwan University of Science and Technology, Taipei, in 2004 and 2009, respectively. From October 2009 to August 2012, he was a Postdoctoral Researcher with the Department of Electrical Engineering, National Taiwan University. He is currently an Associate Professor of electrical engineering with National Taiwan Ocean University, Keelung, Taiwan. His research interests include motor drive control, power electronic applications, and control applications.

YA-WEI YI was born in Keelung, Taiwan, in 1995. He received the B.S. and M.S. degrees in electrical engineering from National Taiwan Ocean University, Keelung, Taiwan, in 2017 and 2019, respectively. He is currently a Senior Design Engineer with Foxconn Electronics Engineering. His research interests include motor drive control and robotics hardware development.